Cosmic Research, Vol. 40, No. 2, 2002, pp. 142–156. Translated from Kosmicheskie Issledovaniya, Vol. 40, No. 2, 2002, pp. 156–170.

Passive Magnetic Attitude Control System for the *Munin* Nanosatellite

M. Yu. Ovchinnikov and V.I. Penkov

Keldysh Institute of Applied Mathematics, Russian Academy of Sciences, Miusskaya pl. 4, Moscow, 125047 Russia

Received March 22, 2000

Abstract—The instrumental and applied problems related to the design of a passive magnetic attitude control system for the *Munin* nanosatellite are considered. The system is constructed from a strong permanent magnet and a set of hysteresis rods. These rods are made of magnetically soft material using a special technology, and they allow us to support the satellite orientation with respect to the local magnetic field vector with a given accuracy and time response. By using asymptotic and numerical methods, we investigate the satellite dynamics for different models of hysteresis. The issues concerning the arrangement of the rods and their interaction with the fields of permanent magnets mounted onboard the satellite are discussed.

INTRODUCTION

When space experiments and investigations aimed to study the magnetosphere, ionosphere, the behavior of charged particles and other phenomena in the geomagnetic field are carried out, the orientation of the satellite longitudinal axis along the vector **H** of the local geomagnetic field is most preferable. Adjusting the axes of instrument sensitivity along this orientation axis or in a given position relative to it, one can provide for a fixed position of measuring instruments with respect to the objects of investigation. Such a mode of angular motion is the most suitable for a small satellite, since for a large spacecraft usually there is a possibility to install instruments on a movable platform with an autonomous system of sighting onto the observed objects or phenomena. Small spacecraft do not have this possibility for many reasons, primarily because of limitations in weight, size, and power.

Several years ago the Institute of Space Physics (Kiruna, Sweden) approved the project of a nanosatellite called *Munin*[1] in order to demonstrate the capability of so small a satellite to solve real scientific problems. The *Munin* satellite [1] with a mass of 6 kg should bear a combined spectrometer of electrons and ions MEDUSA (this instrument was first tested during the flight of the *Astrid-2* microsatellite) and a solid state detector DINA. It is also anticipated that the data on auroral effects in the upper layers of the Earth's atmosphere and ionosphere will be collected in the Northern and Southern hemispheres in such a manner that the data on the current state of the magnetosphere be available in the real time mode through the Internet. For this purpose, it is planned to make photos of auroras with the help of a miniature CCD-camera in the visible light and UV ranges. This chamber has a field of view 32° wide, its resolution is 340×240 pixels ($0.2 \times 0.2°$), the scale of gray includes 64 digitization levels, and the minimum exposure is 1/1000 s, while the operating exposure is 0.5–1 s in the range 450–800 nm. In addition, two single-axis magnetometers are installed on the satellite, and there is a possibility to control the output currents of six panels of solar batteries. The arrangement of the instruments inside the satellite and its external view without the panels of solar batteries are shown in Fig. 1. The satellite is cubic in form with edges 21-cm long. The panels of silicon solar batteries cover all six facets of the cube, providing for 4 W of mean electric power at a voltage of 15–20 V. Together with a lithium ionic buffer battery, peak power during the transmitter operation can reach 11.6 W. Satellite communication with the flight control ground station in Kiruna, Sweden, is implemented in the UHF range. A digital processor unit controls all the instruments and provides for compressing the data and formatting the telemetric information. It is also used for modem control. According to the existing classification, this satellite can be included in the category of nanosatellites whose mass lies in the range from 1 to 10 kg [2]. *Munin* was successfully launched in its orbit on November 21, 2000, as a co-payload.

Based on the requirements of the scientific instrumentation, the most preferable mode of the angular motion of the *Munin* satellite is the orientation of its longitudinal axis along the **H** vector. In this case, it remains to be clarified what type of magnetic system is preferable for the satellite under consideration. The solution to this problem is determined by the requirements of the satellite angular motion and of its mass-size and energy characteristics. The satellite does not

[1] According to Scandinavian mythology, the ravens Munin and Hugin used to fly all over the world to collect news. Sitting on the shoulders of the supreme god Odin, they whispered the news in his ears. Munin and Hugin, respectively, were the personified memory and intellect of Odin. Together, they were an embodiment of his soul.

0010-9525/02/4002-0142$27.00

require high-precision orientation and complicated programmed maneuvers during the flight, while there is no possibility of installing active executing devices and attitude control sensors. Deviation from **H** should not exceed 10°–15° during the entire time of flight. The tolerable time of reaching the nominal motion must be no more than two–three weeks. The system should not include movable magnetic elements, and it should not consume energy and information resources of the satellite. Finally, the system should be as cheap as possible. Therefore, the choice of the type of the attitude control system is unambiguously completed by a passive magnetic system.

Two principal problems that should be solved in designing a passive magnetic system of a satellite's attitude control are to provide for restoring and damping moments. The problem of restoring moment is solved by a permanent magnet whose axis is aligned with the oriented axis. In order to solve the second problem, a damping device is required for dissipation of the energy of angular motion. The ways to solve the problem of dissipating the energy of a satellite's perturbed attitude motion and the methods of their implementation are discussed in detail in [3]. The damping device chosen for the *Munin* satellite consists of a set of hysteresis rods made from a magnetically soft material. These rods reverse their magnetization in the geomagnetic field when the satellite rotates relative to the **H** vector. Let us consider the problems arising when a permanent magnet and hysteresis rods are used for developing an attitude control system.

Due to the nonuniform rotation of the **H** vector in the inertial space and its changing magnitude when the satellite's center of mass moves along the orbit, it is impossible in principle to provide for an exact orientation of the longitudinal axis of the satellite. Mathematically, this fact reveals itself in the inhomogeneity of equations describing the satellite's oscillations with respect to **H**, because of the noninertiality of the coordinate system in which the satellite motion is considered. One can only reduce the amplitude of forced oscillations. The presence of forced oscillations results in the hazard of the occurrence of external and internal resonances.

The hysteresis rods from magnetically soft material damp both rotational and oscillatory motions of a satellite with respect to the **H** vector, but they require a meticulous mathematical simulation of hysteresis and satellite dynamics when the parameters of the rods are determined. In addition, rather strict requirements of the arrangement of the attitude control system in the satellite body should be met. When manufacturing the rods, it is necessary to find the appropriate magnetic material and to observe strictly the technological process.

Fairly sophisticated precession motions of the satellite about the **H** vector are possible, in which the rods change their magnetization in particular hysteresis loops. As a result, the satellite slowly reaches stationary motion, i.e., the duration of the transition process increases. The possibility for a satellite to reach such modes of motion depends on the relationship between satellite's moments of inertia and on the initial conditions of its motion.

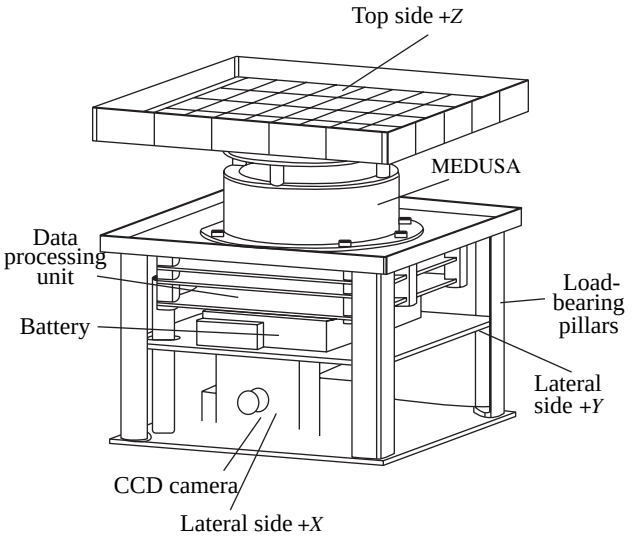

Fig. 1. Arrangement of instruments inside the *Munin* satellite.

Transition motions of a satellite with a magnetic system of attitude control were considered in [4], using a simple model of hysteresis and the method of averaging, for small deviations of the orientation axis aligned with a permanent magnet. In this case, assuming the influence of hysteresis rods on the stationary motion to be small as compared to disturbances from the magnetic field nonuniformity, one can consider periodic motions of the satellite with a permanent magnet as stationary [5].

It should be noted that passive magnetic systems of attitude control have been sufficiently widely used and are still in use for maintaining autonomous orientation of small-size satellites. Here are some of them that were successfully launched: *Transit-1B* (1960), *Transit-2A* (1960), *Injun-3* (1962), *ESRO-1A* (1968), *ESRO-1B* (1969), *Azur* (1969), *Exos* (1978), *Magion* (1978). A short description of these projects is given in [3]. Four microsatellites *Microsat-NA* (1990) are described in [6]. Four picosatellites *JAK*, *Thelma*, *Louise*, and *Stensat* with a mass of several hundred grams were launched in 2000 [7].

1. FORMULATION OF THE PROBLEM: EQUATIONS OF MOTION

In its inertial properties, the *Munin* satellite is close to a dynamically symmetric solid body. So we consider a dynamically axisymmetric solid body with a permanent magnet and hysteresis rods from a magnetically soft material. Let us assume the dipole moment of the

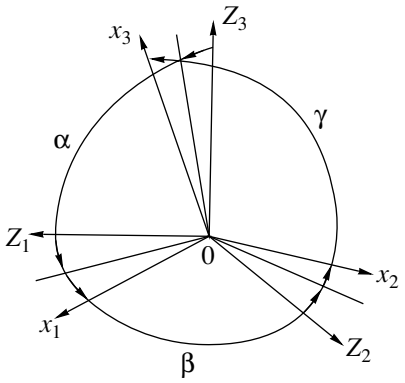

Fig. 2. Satellite-fixed and magnetic coordinate systems.

permanent magnet to be parallel to the satellite's axis of symmetry, while the hysteresis rods are located perpendicular to the dipole moment of the permanent magnet. The advantage of such a position of the rods is substantiated in [4]. The satellite's center of mass moves along a circular orbit around the Earth. To write the equations of motion of the satellite relative to its center of mass we introduce three rectangular systems of coordinates:

$Ox_1x_2x_3$ is the satellite-fixed system of coordinates. The point O is the center of mass of the satellite, the axes Ox_1, Ox_2, and Ox_3 are the principal central axes of inertia; and the dipole moment of the permanent magnet is parallel to the Ox_1 axis.

$OX_1X_2X_3$ is the orbital system of coordinates. The OX_3 axis is directed along the geocentric radius vector of the point O. The OX_2 axis is parallel to the orbit plane. The OX_1 axis is codirected with the satellite motion.

$OZ_1Z_2Z_3$ is the magnetic system of coordinates related to the vector **H** of the geomagnetic field strength at the point O. The unit vectors $\mathbf{s}_1$, $\mathbf{s}_2$, and $\mathbf{s}_3$ of this system have the form

$$\mathbf{s}_1 = \frac{\mathbf{H}}{|\mathbf{H}|}, \quad \mathbf{s}_3 = \frac{\mathbf{s}_1 \times \mathbf{E}_2}{|\mathbf{s}_1 \times \mathbf{E}_2|}, \quad \mathbf{s}_2 = \mathbf{s}_3 \times \mathbf{s}_1,$$

where $\mathbf{E}_2$ is the unit vector of the OX_2 axis. Such a choice of unit vectors is suitable for near-polar orbits.

Let us specify the position of the $OX_1X_2X_3$ coordinate system relative to the $OZ_1Z_2Z_3$ system by the angles α, β, and γ (Fig. 2). The elements of the corresponding transition matrix $\|b_{jn}\|$ have the form $b_{jn} = \cos(Z_j, x_n)$ $j, n = 1, 2, 3$. We write the elements $h_{jn} = \cos(X_j, Z_n)$ (where $j, n = 1, 2, 3$) of the matrix $\|h_{jn}\|$ of transition from the $OZ_1Z_2Z_3$ system to the $OX_1X_2X_3$ system and the projections $\omega_0\Phi_1$, $\omega_0\Phi_2$, and $\omega_0\Phi_3$ of the absolute angular velocity of the magnetic coordinate system onto its axes as follows:

$$h_{11} = \frac{\sin i \cos u}{N}, \quad h_{12} = -\frac{\cos i \cos u}{NN_1},$$

$$h_{13} = \frac{\sin u}{N_1}$$

$$h_{21} = \frac{\cos i}{N}, \quad h_{22} = \frac{N_1 \sin i}{N}, \quad h_{23} = 0,$$

$$h_{31} = -\frac{\sin i \sin u}{N}, \quad h_{32} = \frac{\cos i \sin u}{NN_1},$$

$$h_{33} = \frac{\cos u}{N_1};$$

$$\Phi_1 = \frac{3(1 + \sin^2 u)\cos i}{NN_1^2},$$

$$\Phi_2 = \frac{3(1 + \sin^2 u)\sin i}{NN_1}; \quad \Phi_3 = -\frac{3\sin 2u \sin 2i}{4N^2 N_1},$$

where $N = \sqrt{1 + 3\sin^2 i \sin^2 u}$, $N_1 = \sqrt{1 + 3\sin^2 u}$, u is the latitude argument, i is the orbit inclination, and ω_0 is the angular velocity of the orbital motion of the satellite's center of mass. The model of the *right dipole* is accepted for description of the geomagnetic field.

Out of the external moments acting upon the satellite we take into account the gravitational moment and two magnetic moments: restoring (produced by a permanent magnet) and damping (produced by hysteresis rods). In this case, the equations of motion for an axisymmetric ($B = C$) satellite in a circular orbit relative to its center of mass have the following form:

$$\begin{aligned}
A\frac{d\omega_1}{dt} &= \mu_0 H V_b \overline{W}(e_2 b_{13} - e_3 b_{12}),\\
B\frac{d\omega_2}{dt} + (A - B)\omega_3\omega_1 &= 3\omega_0^2(A - B)\xi_3\xi_1\\
&+ \mu_0 H V_b \overline{W}(e_3 b_{11} - e_1 b_{13}) - \mu_0 m H b_{13},\\
B\frac{d\omega_3}{dt} + (B - A)\omega_1\omega_2 &= 3\omega_0^2(B - A)\xi_1\xi_2\\
&+ \mu_0 H V_b \overline{W}(e_1 b_{12} - e_2 b_{11}) + \mu_0 m H b_{12},\\
\frac{\gamma}{dt} &= \bar{\omega}_1 - (\bar{\omega}_2\cos\gamma - \bar{\omega}_3\sin\gamma)\tan\beta,\\
\frac{d\alpha}{dt} &= \frac{1}{\cos\beta}(\bar{\omega}_2\cos\gamma - \bar{\omega}_3\sin\gamma),\\
\frac{d\beta}{dt} &= \bar{\omega}_2\sin\gamma + \bar{\omega}_3\cos\gamma.
\end{aligned} \tag{1}$$

Here, A and B are the axial and equatorial moments of inertia; ω_1, ω_2, ω_3 are the projections of the vector of the satellite's absolute angular velocity onto the satellite-fixed axes Ox_1, Ox_2, Ox_3; $H_0 = \mu_m/(4\pi r^3)$; $\mu_m = 8.06 \times 10^{22}$ A m^2 is the magnetic moment of the Earth's dipole; r is the radius of the orbit; V_b is the volume of a hysteresis rod; $\mu_0 = 4\pi \times 10^{-7}$ H/m is the magnetic constant; $\overline{W}(\dot{\bar{H}}_\tau, \bar{H}_\tau)$ is the hysteresis function describing the rod magnetization and depending on the material, length-to-diameter ratio, and the external field strength;

$\bar{H}_\tau = (\mathbf{H}, \mathbf{e})$, $(e_1, e_2, e_3)_x$ is the unit vector of the rod longitudinal axis in projections onto the axes Ox_1, Ox_2, and Ox_3; m is the magnitude of the dipole moment $\mathbf{m}$ of the magnet installed on the satellite; t is time; $\bar{\omega}_j = \omega_j - \omega_0 \sum_{n=1}^{3} \Phi_n b_{nj}$ (j =1, 2, 3) are the projections of the vector of satellite's angular velocity relative to the magnetic coordinate system; and $\xi_j = \sum_{n=1}^{3} h_{3n} b_{nj}$ are the components of the unit vector of axis OX_3 in the $Ox_1x_2x_3$ coordinate system. The SI system of units is used. Note that in (1), interactions of the hysteresis rods with the permanent magnet field and with each other are not taken into account. The equations are written taking the action of a single hysteresis rod into account. For several rods, one needs to take a sum of the moments of their interaction with the geomagnetic field in the right hand sides of Eqs. (1).

When studying the satellite's dynamics by the method of averaging, we use the *Rayleigh model* according to which

$$\bar{W}(\dot{\bar{H}}_\tau, \bar{H}_\tau) = (\mu_{in} + \alpha_R \bar{H}_{\tau m})\bar{H}_\tau - \frac{\alpha_R}{2}(\bar{H}_{\tau m}^2 - \bar{H}_\tau^2)\operatorname{sgn}\frac{d\bar{H}_\tau}{dt},$$

where μ_{in} is the initial magnetic permeability, α_R is the Rayleigh constant, and $H_{\tau m}$ is the amplitude of the reversal magnetization field. This model gives the right behavior of the hysteresis loop in the neighborhood of the coordinate origin at a symmetrical reversal magnetization of the rod. This is true for both the loop form and the dependence of its area on the reversal magnetization field amplitude. The application of this model can be considered as a further step as compared to the *parallelogram model* used in [4].

Now let us introduce the following dimensionless parameters

$$\lambda = \frac{A}{B},\ \eta = \frac{\mu_0 m H_0}{B\omega_0^2},\ \varepsilon = \frac{\mu_0 \alpha_R V_b H_0^3}{B\omega_0^2},\ \nu = \frac{\mu_{in}}{\alpha_R H_0}$$

and variables

$$\Omega_1 = \frac{\omega_1}{\omega_0},\quad u = \omega_0(t - t_0),$$

$$\Omega_2 = \frac{1}{\omega_0}(\omega_2\cos\gamma - \omega_3\sin\gamma),$$

$$\Omega_3 = \frac{1}{\omega_0}(\omega_2\sin\gamma + \omega_3\cos\gamma)$$

and rewrite system (1) in the dimensionless form

$$\dot{\Omega}_1 = \frac{\varepsilon\sqrt{1-e_1^2}}{\lambda}NW(\sin\alpha\cos z + \cos\alpha\sin\beta\sin z),$$

$$\dot{\gamma} = \Omega_1 - \Omega_2\tan\beta - \Pi_2/\cos\beta,$$

$$\dot{\Omega}_2 = -(\lambda\Omega_1 - \Omega_2\tan\beta - \Pi_2/\cos\beta)\Omega_3 - \eta N\sin\alpha - 3(1-\lambda)\Lambda_1(\Lambda_2\cos\beta + h_{32}\sin\beta) + \varepsilon NW(\sqrt{1-e_1^2}\cos\alpha\cos\beta\sin z - e_1\sin\alpha), \quad (2)$$

$$\dot{\Omega}_3 = (\lambda\Omega_1 - \Omega_2\tan\beta - \Pi_2/\cos\beta)\Omega_2 - \eta N\cos\alpha\sin\beta + 3(1-\lambda)(\Lambda_2\cos\beta + h_{32}\sin\beta)(-\Lambda_2\sin\beta + h_{32}\cos\beta) - \varepsilon NW(\sqrt{1-e_1^2}\cos\alpha\cos z + e_1\sin\beta)\cos\alpha,$$

$$\dot{\alpha} = \Omega_2/\cos\beta + \Pi_2\tan\beta - \Phi_2,\quad \dot{\beta} = \Omega_3 - \Pi_1.$$

Here, $N = H/H_0$, $H_\tau = \bar{H}_\tau/H_0$,

$$\Pi_1 = \Phi_1\sin\alpha + \Phi_3\cos\alpha,$$

$$\Pi_2 = \Phi_1\cos\alpha - \Phi_3\sin\alpha,$$

$$\Lambda_1 = h_{31}\sin\alpha + h_{33}\cos\alpha,$$

$$\Lambda_2 = h_{31}\cos\alpha - h_{33}\sin\alpha,$$

$$\dot{z} = \gamma + \varphi,\ \sin\varphi = e_3/\sqrt{1-e_1^2},\ \cos\varphi = e_2/\sqrt{1-e_1^2},$$

$$W(\dot{H}_\tau, H_\tau) = (\nu + H_{\tau m})H_\tau - \frac{1}{2}(H_{\tau m}^2 - H_\tau^2)\operatorname{sgn}\frac{dH_\tau}{du}.$$

2. AVERAGING OF EQUATIONS OF MOTION

Let us assume that the magnet installed on the satellite is strong, so that the restoring moment is the governing factor in the satellite motion. This allows us to introduce a small dimensionless parameter $\delta = 1/\sqrt{\eta} \ll 1$ and to change for a *fast time* $\tau = (u - u_0)/\delta$, where u_0 is the latitude argument value which corresponds to the initial instant of the dimensionless time τ. We assume that the proper axial rotation is sufficiently slow ($\Omega_1 \sim 1$). Let us designate the operation of differentiation with respect to τ by a stroke. We will follow the method of analyzing the equations of motion that was used in [4]. Rewrite Eqs. (1) in the fast time τ. At $\delta = 0$, these equations describe the motion of a solid body in the Lagrange case, admitting the known three first integrals

$$\Omega_1 = C_1,$$

$$(\alpha'\cos\beta)^2 + (\beta')^2 - N\cos\alpha\cos\beta = C_2,$$

$$\alpha'\cos\alpha\sin\beta\cos\beta - \beta'\sin\alpha = C_3,$$

where C_j are some constants (j = 1, 2, 3).

In a particular case, the solution to the equations in the fast time has the form Ω_1 = const, γ = const, $\alpha = \beta =$ 0. Let us make a change of variables $\alpha = \delta\bar{\alpha}$, $\beta = \delta\bar{\beta}$. Retaining the first nonzero terms in the expansion in terms of integer nonnegative powers of the parameter δ, we arrive at the system of equations

$$\Omega_1' = \delta^2\frac{\varepsilon\sqrt{1-e_1^2}}{\lambda}NW(\bar{\alpha}\cos z + \bar{\beta}\sin z),$$

$$\gamma' = \delta(\Omega_1 - \Phi_1), \quad (3)$$

$$\bar{\alpha}'' + N\bar{\alpha} = \delta G_1,\quad \bar{\beta}'' + N\bar{\beta} = \delta G_2,$$

where

$$G_1 = (-\lambda\Omega_1 + 2\Phi_1)\bar{\beta}' - 3(1-\lambda)h_{31}h_{33} - \dot{\Phi}_2 - (\lambda\Omega_1 - \Phi_1)\Phi_3 + \varepsilon NW\sqrt{1-e_1^2}\sin z,$$

$$G_2 = -(-\lambda\Omega_1 + 2\Phi_1)\bar{\alpha}' - 3(1-\lambda)h_{31}h_{32} - \dot{\Phi}_3 - (\lambda\Omega_1 - \Phi_1)\Phi_1 - \varepsilon NW\sqrt{1-e_1^2}\cos z,$$

$$H_\tau' = N[e_2(\bar{\alpha}'\sin\gamma - \bar{\beta}'\cos\gamma) + e_3(\bar{\alpha}'\cos\gamma + \bar{\beta}'\sin\gamma)]$$

are the functions that were obtained as a result of this change of variables. At $\delta = 0$, the last two equations in (3) admit the following solution

$$\bar{\alpha} = A_1\cos\psi_1, \quad \bar{\alpha}' = -\rho A_1\sin\psi_1, \qquad \bar{\beta} = A_2\cos\psi_2, \quad \bar{\beta}' = -\rho A_2\sin\psi_2, \tag{4}$$

where $\psi_j = \rho\tau + \zeta_j$ ($j = 1, 2$); A_j and ζ_j are the integration constants; and $\rho = \sqrt{N}$.

For conversion from the variables $\bar{\alpha}$, $\bar{\beta}$, $\bar{\alpha}'$, $\bar{\beta}'$ (4) to the variables A_1, A_2, ψ_1, ψ_2, let us use formulas (4). Resolving the equations derived as a result of these transformations for derivatives, we derive the following system of equations in a standard form, ready for the Krylov–Bogolyubov method of averaging to be used

$$A_j' = -\delta(\dot{\rho}A_j\sin\psi_j + G_j)(\sin\psi_j)/\rho,$$

$$\psi_j' = \rho - \delta(\dot{\rho}\sin\psi_j + G_j/A_j)(\cos\psi_j)/\rho \quad (j = 1, 2),$$

$$\Omega_1' = \delta^2\varepsilon NW\sqrt{1-e_1^2} \times (A_1\cos\psi_1\cos z + A_2\cos\psi_2\sin z)/\lambda,$$

$$\gamma' = \delta(\Omega_1 - \Phi_1); \tag{5}$$

$$H_\tau' = \rho N\sqrt{1-e_1^2}(-A_1\sin\psi_1\sin z + A_2\sin\psi_2\cos z).$$

The frequencies of changing fast variables ψ_1 and ψ_2 are coincident in the asymptotic sense and are equal to ρ. Following the Krylov–Bogolyubov scheme of averaging for a resonance case, we introduce the variable θ as a phase difference

$$\theta = \psi_2 - \psi_1. \tag{6}$$

Let us express ψ_2 from (6) and substitute it into system (5). As a result of transformations we get the following equations

$$A_1' = -\delta(\dot{\rho}A_1\sin^2\psi_1 + \bar{G}_1\sin\psi_1)/\rho,$$

$$A_2' = -\delta[\dot{\rho}A_2\sin^2(\psi_1 + \theta) + \bar{G}_2\sin(\psi_1 + \theta)]/\rho,$$

$$\theta' = -\delta[\bar{G}_2\cos(\psi_1 + \theta)/A_2 - \bar{G}_1\cos\psi_1/A_1]/\rho,$$

$$\Omega_1' = \delta^2\varepsilon\sqrt{1-e_1^2}NW \times [A_1\cos\psi_1\cos z + A_2\cos(\psi_1 + \theta)\sin z]/\lambda,$$

$$\gamma' = \delta(\Omega_1 - \Phi_1). \tag{7}$$

Here,

$$\bar{G}_1 = G_j|_{\psi_2 = \psi_1 + \theta} \quad (j = 1, 2),$$

$$\sin\psi_1^* = A_2\cos z\sin\theta/\Phi$$

$$\cos\psi_1^* = (-A_1\sin z + A_2\sin z\cos\theta)/\Phi,$$

$$H_\tau' = \rho N\sqrt{1-e_1^2}\Phi\sin(\psi_1 + \psi_1^*),$$

$$\Phi = \sqrt{A_1^2\sin^2 z + A_2^2\cos^2 z - A_1A_2\sin 2z\cos\theta}.$$

Applying the Krylov–Bogolyubov method of averaging, which was adapted for equations with discontinuous right hand sides in [8], we construct the solution to system (7) in the form

$$y = \bar{y} + \delta Y(\bar{y}, u_0, \delta), \tag{8}$$

where $y = (\Omega_1, \gamma, A_1, A_2, \theta)$ is the vector of slow variables, $\bar{y} = (\bar{\Omega}_1, \bar{\gamma}, \bar{A}_1, \bar{A}_2, \bar{\theta})$ is the vector of new variables, and Y is the unknown vector-function. Then, for new variables $\bar{y}$ under the first approximation in the small parameter δ, we have the vector equation

$$\bar{y}' = \delta\bar{Y}. \tag{9}$$

Here, $\bar{Y}$ is the vector function of the right hand sides of system (7), which are related to the δ parameter and averaged over the fast phase ψ_1 on the interval $(0, 2\pi)$. In what follows, we will omit the overline above the new slow variables.

In spite of the fact that we do not take into account the influence of the strong permanent magnet on the hysteresis rods, it is reasonable to consider only such configurations in which the rod lies in the equatorial plane of the permanent magnet; i.e., $e_1 = 0$. In this case, the component of the vector of field strength of a permanent magnet along the hysteresis rod is close to zero, and the working point remains nondisplaced.

Averaging the right hand sides of equations (7) in ψ_1, changing back for the independent variable u, and designating $\chi = (2\Phi_1 - \lambda\Omega_1)/2$, we arrive at the following equations:

$$\dot{A}_1 = -\frac{\dot{\rho}A_1}{2\rho} + \chi A_2\cos\theta - \frac{\varepsilon\delta N^2\sin z}{2\rho}\left[\nu A_2\cos z\sin\theta + \delta N\Phi \times\left(\frac{4}{3\pi}A_1\sin z - A_2\cos z\left(\frac{4}{3\pi}\cos\theta - \sin\theta\right)\right)\right],$$

$$\dot{A}_2 = -\frac{\dot{\rho}A_2}{2\rho} - \chi A_1\cos\theta$$

$$+\frac{\varepsilon\delta N^2\cos z}{2\rho}\Big[\nu A_1\sin z\sin\theta+\delta N\Phi$$
$$\times\Big(A_1\sin z\Big(\sin\theta+\frac{4}{3\pi}\cos\theta\Big)-\frac{4}{3\pi}A_2\cos z\Big)\Big],$$
$$\dot\theta=-\Big\{\chi\Big(\frac{A_2}{A_1}-\frac{A_1}{A_2}\Big)+\frac{\varepsilon\delta N^2}{2\rho^2}$$
$$\times\Big[\nu\Big(\cos 2z+\sin z\cos z\cos\theta\Big(\frac{A_2}{A_1}-\frac{A_1}{A_2}\Big)\Big)\qquad(10)$$
$$+\delta N\Phi\Big(\cos 2z+\sin z\cos z$$
$$\times\Big(\frac{4}{3\pi}\sin\theta\Big(\frac{A_2}{A_1}+\frac{A_1}{A_2}\Big)+\cos\theta\Big(\frac{A_2}{A_1}-\frac{A_1}{A_2}\Big)\Big)\Big)\Big]\Big\},$$
$$\dot\Omega_1=\frac{\varepsilon\delta^2N^2}{2\lambda}$$
$$\times[\nu((A_1^2-A_2^2)\sin z\cos z-A_1A_2\cos\theta\cos 2z)$$
$$+\delta N\Phi\Big((A_1^2-A_2^2)\sin z\cos z$$
$$-A_1A_2\Big(\cos 2z\cos\theta+\frac{4}{3\pi}\sin\theta\Big)\Big)\Big],$$
$$\dot z=\Omega_1-\Phi_1,$$

where the right hand sides of the equations are written accurate to $O(\delta)$, except for the last equation which is accurate to $O(\delta^2)$.

2.1. Two Identical Mutually Orthogonal Rods

Let two identical mutually orthogonal rods be installed on the satellite. Then system (10) assumes the form

$$\dot A_1=-\frac{\dot\rho A_1}{2\rho}+\chi A_2\cos\theta$$
$$-\frac{\bar\varepsilon N^3}{2\rho}\Big[\frac{4}{3\pi}A_1(\Phi_{(1)}\sin^2z+\Phi_{(2)}\cos^2z)$$
$$-A_2\sin z\cos z(\Phi_{(1)}-\Phi_{(2)})\Big(\frac{4}{3\pi}\cos\theta-\sin\theta\Big)\Big],$$
$$\dot A_2=-\frac{\dot\rho A_2}{2\rho}-\chi A_1\cos\theta$$
$$+\frac{\bar\varepsilon N^3}{2\rho}\Big[A_1\sin z\cos z(\Phi_{(1)}-\Phi_{(2)})\Big(\sin\theta+\frac{4}{3\pi}\cos\theta\Big)$$
$$-\frac{4}{3\pi}A_2(\Phi_{(1)}\cos^2z+\Phi_{(2)}\sin^2z)\Big],$$
$$\dot\theta=-\Big\{\chi\Big(\frac{A_2}{A_1}-\frac{A_1}{A_2}\Big)+\frac{\bar\varepsilon N^3}{2\rho}(\Phi_{(1)}-\Phi_{(2)})\qquad(11)$$
$$\times\Big[\cos 2z+\sin z\cos z\Big(\frac{4}{3\pi}\sin\theta\Big(\frac{A_2}{A_1}+\frac{A_1}{A_2}\Big)$$
$$+\cos\theta\Big(\frac{A_2}{A_1}-\frac{A_1}{A_2}\Big)\Big)\Big]\Big\},$$
$$\dot\Omega_1=\frac{\bar\varepsilon N^3}{2\lambda}\Big[(\Phi_{(1)}-\Phi_{(2)})$$
$$\times[(A_1^2-A_2^2)\sin z\cos z-A_1A_2\cos 2z\cos\theta]$$
$$-\frac{4}{3\pi}A_1A_2(\Phi_{(1)}+\Phi_{(2)})\sin\theta\Big],$$
$$\dot z=\Omega_1-\Phi_1,$$

where

$$\Phi_{(1)}=\sqrt{A_1^2\sin^2z+A_2^2\cos^2z-A_1A_2\sin 2z\cos\theta},$$
$$\Phi_{(2)}=\sqrt{A_1^2\cos^2z+A_2^2\sin^2z+A_1A_2\sin 2z\cos\theta},$$
$$\bar\varepsilon=\varepsilon\delta^2.$$

It follows from system (11) that the installation of two identical mutually orthogonal rods in the magnet's equatorial plane leads to mutual cancellation of the terms proportional to ν. These terms represent the intensity of magnetization that is linearly dependent on the strength of the field applied to the rods. The role they play by disturbing the satellite motion is parasitic. Only those terms remain in the equations that are determined by nonlinear magnetization and by a displacement of the magnetization curve due to hysteresis.

In the case $\bar\varepsilon=0$, system (10) has three first integrals c_1, c_2, and c_3 derived in [9] and [10]. Let us rewrite expressions for A_1, A_2, and θ using the three first integrals

$$\rho(A_1^2+A_2^2)=c_1,\quad 2\rho A_1A_2\sin\theta=c_2,$$
$$\cot\theta=\sqrt{p^2-1}\sin(s+c_3),\qquad(12)$$

where $p=c_1/c_2$, $s=2\int_0^u\chi\,du$; in the following form

$$A_1^2=\frac{1}{2\rho}[c_1-\sqrt{c_1^2-c_2^2}\cos(s+c_3)],$$
$$A_2^2=\frac{1}{2\rho}[c_1+\sqrt{c_1^2-c_2^2}\cos(s+c_3)].\qquad(13)$$

Here, $\Phi=\{[c_1+(c_1^2-c_2^2)^{1/2}\cos(s+c_3+2z)]/(2\rho)\}^{1/2}$. Let us take c_1, c_2, and c_3 as new variables at $\bar\varepsilon\neq 0$. In order to make a conversion from variables A_1, A_2, and θ in system (11) to the new variables c_1, c_2, and c_3 we use

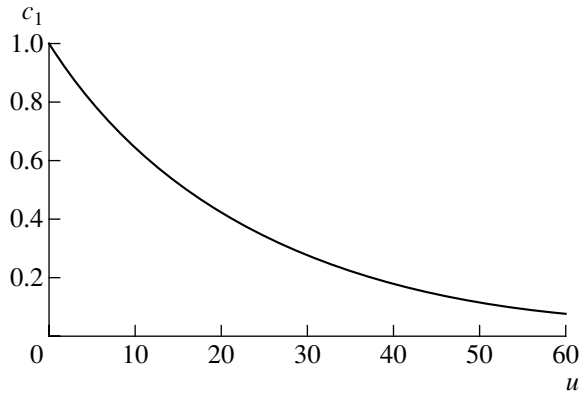

Fig. 3. The c_1 behavior versus u at $i = \pi/2$.

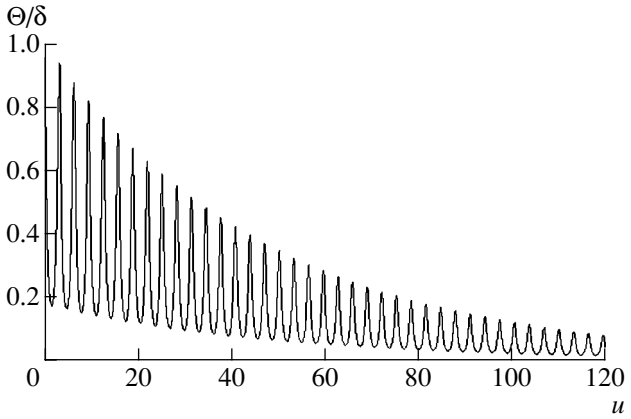

Fig. 4. Dependence of the Θ angle on u at $i = \pi/2$.

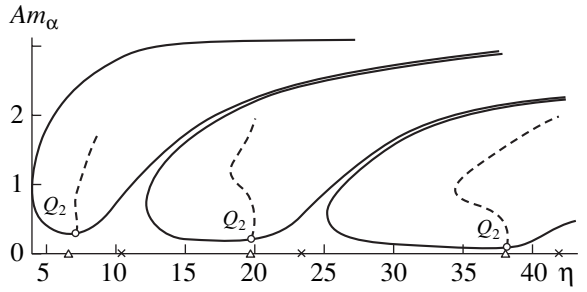

Fig. 5. Amplitude characteristics of forced periodic motions of a satellite in the plane of a polar orbit.

relations (12) and (13). As a result of some transformations, we have

$$\dot{c}_1 = -\bar{\varepsilon}\frac{4}{3\pi}\frac{N^3}{\rho}c_1, \quad \dot{c}_2 = -\frac{\bar{\varepsilon}c_2}{\rho\Phi},$$
$$\dot{c}_3 = \frac{\bar{\varepsilon}c_1\sin(s + c_3 + 2z)}{\rho\Phi(c_1^2 - c_2^2)^{1/2}}. \qquad (14)$$

Take a notice that the equation for c_1 is isolated and does not contain the fast variable z. This allows the solution for c_1 to be written below in the form of a quadrature.

Let $0 < \bar{\varepsilon} \ll 1$. Generally speaking, we should average the right hand sides of equations (14) over the fast variable z. The first equation does not contain the z variable; therefore, no averaging is required. Integrating this equation for c_1 we get its solution in the quadrature form

$$c_1(u) = c_1(u_0)\exp\left(-\frac{4}{3\pi}\bar{\varepsilon}\int_{u_0}^{u}(1 + 3\sin^2 i\sin^2 u)^{5/4}du\right). \qquad (15)$$

Then, the dependence of the angle Θ of the satellite' axis deviation from vector **H** on the latitude argument u is described by the following expression which is derived from (12) and (15):

$$\Theta(u) = \frac{1}{\delta}\frac{\Theta(u_0)}{(1 + 3\sin^2 i\sin^2 u)^{1/8}}$$
$$\times \exp\left(-\frac{2}{3\pi}\bar{\varepsilon}\int_{u_0}^{u}(1 + 3\sin^2 i\sin^2 u)^{5/4}du\right). \qquad (16)$$

According to the Rayleigh model, the area S_h of the hysteresis loop is expressed through the Rayleigh constant α_R and the amplitude of the magnetization field, by the formula $S_h = 16\alpha_R\bar{H}_{rm}^3/3$. For small $\bar{H}_{rm}^3$, the value of α_R remains constant. Therefore, one can determine S_h and calculate α_R from experimental results. The coefficient $\bar{\varepsilon}$ appearing in (16) is defined as $\bar{\varepsilon} = \alpha_R V_b H_0^2/m$. With experimental data on loops available, one can describe quantitatively the transition process by using the above formulas.

Integration of system (11) of the averaged equations and calculation of quadratures (15) and (16) using standard models present no problem whatsoever. Let us give a typical example of numerical calculation of quadratures (15) and (16). For the sake of certainty, we assume $\Theta(0)/\delta = 1$. Two identical mutually orthogonal rods are installed onboard the satellite in the equatorial plane of a permanent magnet. Let the dimensionless parameter $\bar{\varepsilon} = 0.1$. The behavior of c_1 as a function of u and for $c_1(0) = 1$ is shown in Fig. 3. The plot showing the variation of Θ related to δ as a function of u is presented in Fig. 4 for $i = \pi/2$.

The chosen value of the dipole moment of the permanent magnet is 0.3 A m^2. It corresponds to the value of the satellite's dimensionless parameter η equal to 120 and to the value of the δ parameter $\delta \approx 0.09$. What is the meaning of the η parameter? When a satellite passes through the magnetic equator, the quantity $\sqrt{\eta}/2\pi$ is close to the angular frequency of oscillations

Table 1. Magnetic parameters of various satellites

Satellite	Satellite's moment of inertia, kg m^2	Dipole moment of a magnet, A m^2	Magnetic parameter η
Transit-1B	13	0	62
Transit-2A	11.5	?	?
Injun-3	1	140	115
ESRO-1A	9.32	54	117
Azur	8.4	97	233
TTS	0.19	2	212

of the oriented satellite axis with respect to the **H** vector. Near the poles, the frequency increases approximately by a factor of $\sqrt{2}$. The amplitude of forced oscillations of the satellite with respect to the **H** vector decreases inversely proportional to the value of η. Figure 5 is a pictorial rendition of the amplitude of forced periodic oscillations of the satellite's axis of symmetry with respect to the **H** vector in the plane of a polar orbit versus the η parameter [3]. The values of curve points are calculated as $Am_\alpha = \max_{(0 \le u \le \pi)} |\alpha(u)|$, where $\alpha(u)$ is the angle between the vector **H** and the satellite's axis of symmetry. One can see discontinuities due to resonances in the vicinities of which the monotonicity of the decreasing amplitude of the satellite's forced oscillations with the increasing η parameter is violated. The amplitudes of spatial solutions branching at the resonance points Q_2 are shown by dashed lines. The branching points of plane solutions and the points of the spatial motions branching-off from them are shown by the symbols × and Δ. These points are determined by asymptotic formulas. The pattern of branching for plane and spatial motions is described in more detail in [5]. This appears to mean that the increase of η serves to decrease the amplitude. However, in practice it is shown that, starting from amplitudes of the order of 5°–10°, the main contribution to the amplitude is made by the residual rotation about the orientation axis and by the uncompensated residual magnetic moment of the hysteresis rods. Increasing η does not promote the reduction of these factors, since the smaller the amplitude of oscillations with respect to the **H** vector, the worse the damping of the velocity of proper rotation and the stronger the permanent magnet's influence on the hysteresis rods because of the small dimensions of the satellite. It seems that a magnet with a dipole moment $m = 0.3$ A m^2 ($\eta = 120$) fairly well provides for specified characteristics of the satellite motion. At a polar orbit, the nearest resonance points in the η parameters, where a resonance *in the orbit plane* can take place, are 95 and 130, while for motions *beyond the orbit plane* such points are 92 and 126. The resonance zones in the neighborhood of these points are fairly narrow, and it is possible to check for the occurrence of resonance by direct numerical simulation of the satellite dynamics. Before discussing this numerical simulation, it is necessary to solve the problems of the parameters of the rods and of their arrangement.

3. ESTIMATION OF PARAMETERS OF HYSTERESIS RODS

Now let us present some argumentation allowing the characteristics of the hysteresis rods to be estimated. The satellites that were supplied with the rods are listed above, and we give in Tables 1 and 2 their characteristics. The question mark means that the corresponding quantities were unknown to us.

Unlike the permanent magnet, whose efficiency is practically proportional to its dipole moment value, the efficiency of the rods (i.e., their capacity of damping the initial motion and of producing minimum disturbances in the steady-state motion of a satellite) is determined not only by their volume, but also by the material used, the scheme of their arrangement, by the technique of heat treatment, and, to a considerable degree, by their elongation. By the elongation *p* is meant the ratio of the rod length *l* to its diameter *d*. In particular, the volume of the rods installed onboard the *Transit-2B* satellite was four times less than that on the *Transit-1A* satellite, while the area of the hysteresis loop (it can be used as an estimate of damping efficiency) was larger by a factor of five. The basic distinction between the rods consisted in their elongation: for the *Transit-1B* rods it was two times larger. It is known that there exists an optimum elongation, which depends not only on the rod material, but also on their mutual influence due to the demagnetization effect. Usually, the optimum value of

Table 2. Parameters of hysteresis rods of various satellites

Satellite	Total volume of rods, cm^3	Rod material	Number of rods
Transit-1B	200	AEM 4750	8
Transit-2A	50	AEM 4750	8
Injun-3	50	Permalloy	22
ESRO-1	12	PERMENORM-5000	20
Azur	–	–	8
TTS	2.5	AEM 4750	20

Table 3. Parameters of molybdenum permalloy of the 79NM sort

Initial magnetic permeability $\mu_{r\,in}$	Maximum magnetic permeability $\mu_{r\,max}$	Coercive force H_c, A/m	Saturation induction B_s, T
60000	164000	0.96	0.74

p lies within the limits 200–300. In order make real optimization, one needs the exact mathematical model of hysteresis and a model of the mutual influence of the rods. At this first stage of our research, we restrict ourselves to estimating the required total volume of rods, V_{rod}.

Out of the commercially available magnetically soft materials, we choose one that is easy-to-get, namely, molybdenum permalloy of the 79NM specification. Its composition includes 79% of Ni, 4% of Mo, and 17% of Fe. The characteristics of this material in the form of a strip with a thickness of 1.0 mm are given in Table 3. According to the dipole model of the geomagnetic field, its strength at a circular orbit with a height of 700 km varies from 18.1 A/m up to 36.2 A/m when one moves from the equator to a pole. Even at the maximum strength of the external field, the rod induction is equal to 0.4 T, which is almost two times less than the saturation induction. Therefore, at a complete reversal of magnetization of the rod (along the main loop) one can approximate the main hysteresis loop by a parallelogram. Choosing the arithmetic mean of the maximum and minimum values as the amplitude of the magnetization reversal field and assuming magnetic permeability to be $\mu_{r\,in}$, we obtain for the average area of a hysteresis loop $(\oint H\,dB)_{aver} \approx 8$ T A/m. The approximate equation for the velocity ω of the satellite's rotational motion in the orbit plane has the following form

$$B\frac{d\omega}{dt} = -\frac{1}{2\pi}\left(\oint HdB\right)_{aver}.$$

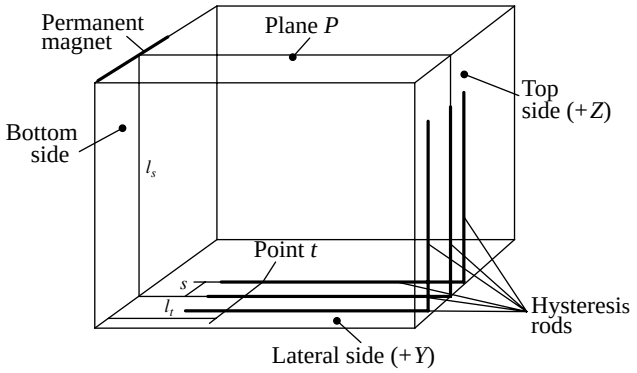

Fig. 6. To calculations of the component $H_{s\tau}$ of vector $\mathbf{H}_s$ along a hysteresis rod displaced from the plane P.

Introducing the initial angular velocity $\omega(0)$, we can write the solution as

$$\omega(t) = \omega(0) - \frac{V_{rod}\left(\oint HdB\right)_{aver}}{2\pi B}t.$$

Hence, it follows that the rotation velocity is damped in a finite time

$$t_{fin} = \frac{2\pi B\omega(0)}{V_{rod}\left(\oint HdB\right)_{aver}}.$$

We assume that several hysteresis rods are installed onboard the satellite (for example, six, in two mutually perpendicular planes of three each). At the 79NM material 0.1 cm thick and for the maximum allowable length of the rods 15.5 cm, we have the volume of one rod V = 0.155 cm^3. Then, for the volume $V_{rod} \sim 0.5$ cm^3 in every plane and at the initial angular velocity $\omega(0) \sim 10$ deg/s, we have as an estimate for the transition process duration $t_{fin} \sim 4$ h. It should be immediately noted that this estimate is very optimistic, more likely there is a lower limit. This is because we did not take into account the real loop area that is appreciably influenced by the proximity of a strong magnet and other magnetized elements of the satellite and its instruments to the rods. Among other unaccounted factors are the satellite's axial rotation, strongly hindering the dissipation of the kinetic energy of rotational motion; the transition process in the satellite's oscillation motion with respect to the **H** vector; and so on. If one refers to the parameters of the *TTS* satellite, which is closest to the *Munin* satellite in its characteristics (see Tables 1 and 2), then one can see that the volume of the *Munin* satellite rods is 2.5 times less, though its moment of inertia is less by a factor of 5.

4. ARRANGEMENT OF HYSTERESIS RODS IN THE SATELLITE'S BODY

As was already mentioned above, the rods must be arranged in the plane that is perpendicular to the axis of the permanent magnet and passes through its center. To make the final choice, we should solve the problem that takes into account the mutual influence of the rods, as well as the influence of the permanent magnet and other magnetized elements of the satellite.

The estimated total volume of the rods $V_{rod} \sim 1$ cm^3 is realized as a pair of triples arranged in mutual perpendicular planes, each rod being 15.5 cm long and 0.1 cm thick at the square cross section. The rods must be arranged in the plane P (Fig. 6), perpendicular to the magnet axis and passing through its center, or, at least, in the planes that are parallel to P and are located not far from it. In this case, the triples should be perpendicular to each other. This means that the ideal place for rods is the intersection of the P plane with the two adjacent lateral faces of the satellite that are the most distant from the permanent magnet. The magnet is located at

the vertex of the dihedral angle composed by two other lateral faces of the satellite. Let us determine the tolerable distance between rods in triples. On the one hand, it is desirable to separate them as far as possible. On the other hand, any displacement from the *P* plane leads to the appearance of the vector $\mathbf{H}_s$ component due to the permanent magnet directed along the rod. The existence of such a component results in the displacement of the working points of the rods, which can adversely affect their efficiency.

Let us derive the expression for the component $H_{s\tau}$ of the vector $\mathbf{H}_s$ directed along the rod. We introduce the following notation (Fig. 6): l_s is the distance from the magnet to the face $S(+Y)$ with the rods; l_t is the distance from the projection O_s of the magnet center onto the face *S* to the projection onto the same face of the point *t* of the rod, in which the component $H_{s\tau}$ is calculated; and *s* is the distance from the point *t* to the plane *P*. Then, under the assumption of the dipole magnetic field of the permanent magnet, we have from corresponding triangles

$$H_{s\tau} = \frac{3msl_t}{4\pi(l_s^2 + l_t^2 + s^2)^{5/2}}.$$

Assuming $s \ll \sqrt{l_s^2 + l_t^2}$ and omitting the terms of the order of $O((s/\sqrt{l_s^2 + l_t^2})^3)$, we rewrite the above expression in the form

$$H_{s\tau} = \frac{3msl_t}{4\pi(l_s^2 + l_t^2)^{5/2}}. \quad (17)$$

It is known [11] that, when the distance between parallel identical rods exceeds 0.3–0.4 of their length, one can disregard their mutual influence. This influence manifests itself in the mutual demagnetization of the rods, and, as a consequence, in a reduced efficiency of damping. At a distance equal to 0.02 of the length, the two rods are practically equivalent to one. At a distance equal to 0.2 of the length, the efficiency is reduced by 12.5%. This means that instead of two rods 1.75 rods will work effectively. We restrict ourselves to the distance of 0.2 lengths and estimate the influence of the permanent magnet field using formula (17). Due to construction limitations on the rod length, the maximum allowable length is $l = 15.5$ cm, hence $s \approx 3$ cm. Three parallel rods are arranged in such a manner that one of them lies on the intersection of the plane *P* with the face *+Z*, while two others lie on the face *+Z* parallel to the first rod at the distances *s* on different sides of it. Another triple of rods will lie on the face *+Y*. According to formula (17), the maximum in l_t value of $H_{s\tau} \approx 0.4$ A/m is reached at $l_t = l_s/2$. All faces of the satellite are assumed to be identical; i.e., the face width is equal to l_s. At the ends of a rod $H_{s\tau} \approx 0.28$ A/m (at $l_t = 4.5$ cm) and $H_{s\tau} \approx 0.25$ A/m (at $l_t = 20$ cm).

Table 4. Curie temperatures of magnetically soft materials

Material sort	Basic composition, %	*T*, °*C*
79NM	79 Ni, 4 Mo, the balance Fe	450
50N	50 Ni, the balance Fe	500

Each rod is placed between two narrow strips (plates) of nonmagnetic material, which are somewhat longer than the rod and have small grooves on their inner sides. A rod in a soft thin envelope is held between these plates with a moderate force. In their turn, the plates are fastened to the satellite body. Such a technique allows the rods to be protected against deformations and mechanical stresses because of the fastening to the satellite body, as well as against vibrations at the stage of launch and thermal deformations during the flight.

Let us analyze the degree of influence of the field strength on the rods. We calculate the coefficient of demagnetization *N* by the approximate empirical formula [11] $N = \ln(1.2p - 1)/p^2$. Substituting into this formula $p = 155$, we get $N = 1.75 \times 10^{-4}$. The magnetic permeability of the *rod* $\mu_r = \mu/(1 + N\mu) \approx 5.5 \times 10^3$, and it weakly depends on the magnetic permeability of the *material* μ. When the magnetic permeability of the material changes from the initial to maximum value, the variation of the magnetic permeability of the rod is only 6%. Therefore, when calculating μ_r we have chosen, for the sake of certainty, the value $\mu \approx 10^5$, which is close to the mean permeability. Now we turn back to the problem of the influence of the magnet field on the hysteresis rods. At a rated steady-state regime, when the amplitude of satellite oscillations with respect to vector **H** is of the order of 0.2 rad, the amplitude of the field demagnetizing the rod is $H_{m\tau} \sim 3.6$ A/m. Comparing this value with the coercive force of the rod material ($H_c = 0.96$ A/m), we conclude that the rod reversal magnetization most probably will go on the limiting loop. The mean projection value $H_{s\tau} \approx 0.3$ A/m results in a

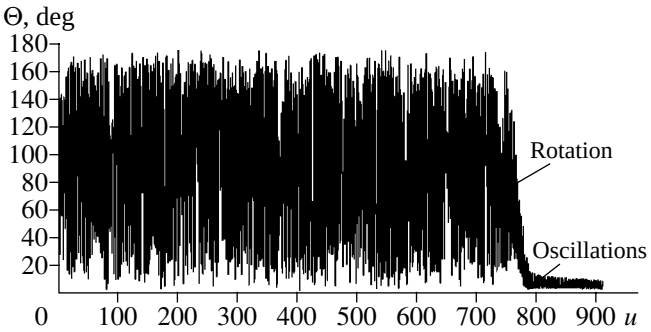

Fig. 7. The angle Θ of deviation of the satellite orientation axis from the **H** vector. The initial angular velocity is equal to $500\omega_0$ in each channel.

Table 5. Parameters of hysteresis rods according to the state standard GOST

Initial magnetic permeability $\mu_{r\,in}$	Maximum magnetic permeability $\mu_{r\,max}$	Coercive force H_c, A/m	Saturation induction B_s, T
25000	180000	1.6	0.74

displacement of the working point by $H_{s\tau}/H_c$, i.e., approximately by 30%, which can be considered as tolerable and lying within the accuracy of modeling.

The permanent magnets of the DINA instrument are another source of parasitic influence on the hysteresis rods. The field intensity of these magnets in the place where the rods are arranged is comparable to the coercive force of the material (H_c = 0.96 A/m), which can result in an extraneous displacement of the working point of the rods and hence in reduction of their efficiency.

The capability of ferromagnets to be magnetized depends on temperature. The magnetizability decreases with increasing temperature: the value of magnetic permeability drops off, the hysteresis effect is weakened, and the saturation magnetization is reduced. At a certain temperature T_K, which is referred to as the Curie temperature, ferromagnetic properties disappear altogether. The Curie temperature is different for different ferromagnets. Table 4 presents the Curie temperatures for some magnetically soft materials most widely used for damping the satellite motions. The molybdenum permalloy 79NM, which is chosen as a rod material, conserves its magnetic properties when the temperature on the panels used for arrangement of the rods aboard the satellite varies within specified limits ±30°C.

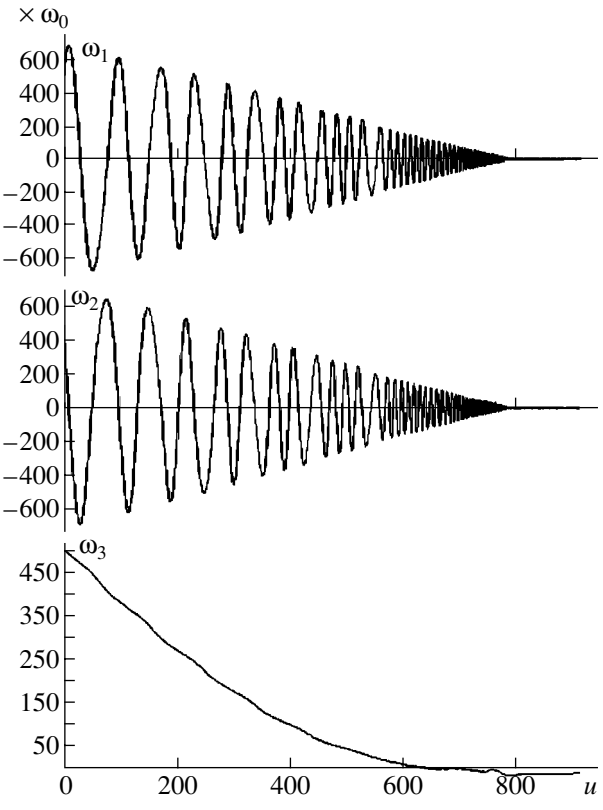

Fig. 8. Projections ω_1, ω_2, and ω_3 of the vector of absolute angular velocity onto the satellite's principal axis of inertia.

5. RESULTS OF NUMERICAL CALCULATIONS

Now we pass on to numerical investigation of the satellite's dynamics under arbitrary initial conditions of motion. It is required to clarify how the characteristics of steady-state and transitional motions of a satellite are influenced by its initial velocity of rotation, the inertia tensor, and the orbit inclination. Three models were used to approximate the geomagnetic field: the right dipole model, the inclined dipole model, and the Gaussian model in the form of an expansion in terms of spherical functions with retaining twelve harmonics (the IGRF-95 model). The attempts to use simple hysteresis models, like the *parallelogram model* or *Rayleigh model*, yield results that are either of a qualitative nature (parallelogram model) or can be used only in the neighborhood of the coordinate origin (Rayleigh model). The complex character of hysteresis requires applying a more sophisticated model. The numerical model of hysteresis used below is known as the *improved model* and described in detail in [12]. Mechanically, this model represents a dilatable rod fixed at one end, lying on a grainy base and rubbing with its lateral surface under the action of a variable tensile force applied to another end. The model proved to yield good results in investigations of the dynamics of the satellites with hysteresis rods. When supplemented by a relatively simple model of the interaction and mutual demagnetization of hysteresis rods [13], this model allows one to choose their basic parameters. When the dynamics were investigated numerically, the kinematic equations included in system (1) were exchanged with Poisson kinematic equations for the first six elements of the matrix $\|b_{jn}\|$

$$\frac{db_{j1}}{dt} = b_{j2}\bar{\omega}_3 - b_{j3}\bar{\omega}_2, \quad \frac{db_{j2}}{dt} = b_{j3}\bar{\omega}_1 - b_{j1}\bar{\omega}_3, \quad \frac{db_{j3}}{dt} = b_{j1}\bar{\omega}_2 - b_{j2}\bar{\omega}_3, \quad (j = 1, 2). \tag{18}$$

The remaining three elements were calculated by the finite formulas

$$b_{31} = b_{12}b_{23} - b_{13}b_{22},$$

$$b_{32} = b_{13}b_{21} - b_{11}b_{23}, \quad b_{33} = b_{11}b_{22} - b_{12}b_{21}.$$

5.1. Results of Preliminary Calculations

First we present the results for a satellite with a spherically symmetric tensor of inertia (the satellite's

moments of inertia are equal to 0.046 kg m^2) and with an orbit inclination of 98°. The satellite bears a permanent magnet with a moment $m = 0.3$ A m^2 oriented parallel to the Ox_1 axis and two triples of rods 15.5 cm long, whose parameters are specified by the state standard GOST (Table 5). The corresponding parameters of the *improved* model of hysteresis are $k = 0.23$, $a = 0.12$, and $R_s = 4.6$. It was demonstrated by a series of calculations that the initial angular velocity of satellite's rotation is the most important factor influencing the duration of transition motion and the orientation accuracy over long-term periods. At the small initial velocity of the order of $50\omega_0$–$100\omega_0$, a satellite reaches the steady-state motion with an amplitude of oscillations with respect to vector **H** equal to 5°–7° for one–two days in every channel (pitch angle, yaw angle, and roll angle).

At the initial angular velocity equal to 30 deg/s or $500\omega_0$, the process of relaxation in any of three channels takes somewhat more than a week, and the satellite executes motion in which the oriented axis moves along a conical surface about the **H** vector with an amplitude of 15°–20°. Then this amplitude slowly decreases to 10°–12° for another couple of days keeping the tendency toward further decreasing. This slow amplitude decrease is due to extremely slow damping of the velocity of the satellite's rotation about the oriented axis. This is caused by the reversal of the magnetization of the rods through the *partial* loops of a fairly small area. This fact was also noted in [14]. An example of the transition process with the initial conditions corresponding to $500\omega_0$ in every channel is given in Fig. 7 (Θ is the angle of deviation of the satellite's orientation axis from the **H** vector) and Fig. 8 (the projections ω_1, ω_2, and ω_3 of the vector of absolute angular velocity onto the satellite's principal axes of inertia) as a function of the dimensionless argument of latitude u; ω_3 is the projection of the absolute angular velocity vector onto the oriented axis. For these initial conditions and satellite parameters, a plot of the angle Θ is presented in Fig. 9 for the orbit number 145. One can clearly see oscillations caused by natural satellite vibrations that are overlapped on slow, almost periodic oscillations with a period close to a half of the orbit period. Here and below, the moments of satellite passage through the equator are marked with an asterisk *. The value of the projection ω_3 of the absolute angular velocity vector was close to $11\omega_0$ in the orbit number 145.

5.2. Final Results of Calculations

Final calculations were carried out with the inertia tensor corresponding to the final configuration of the *Munin* satellite

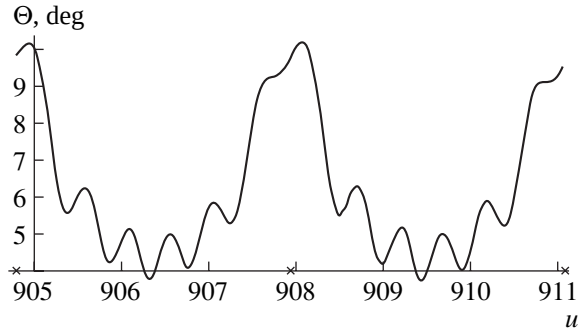

Fig. 9. The angle Θ behavior in the 145th orbit.

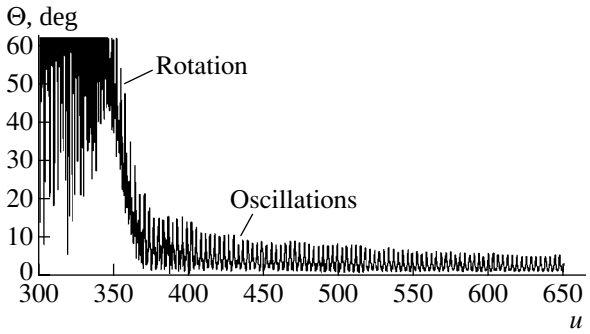

Fig. 10. The angle Θ of deviation of the satellite's orientation axis from the **H** vector. The initial angular velocity is equal to $175\omega_0$ in each channel.

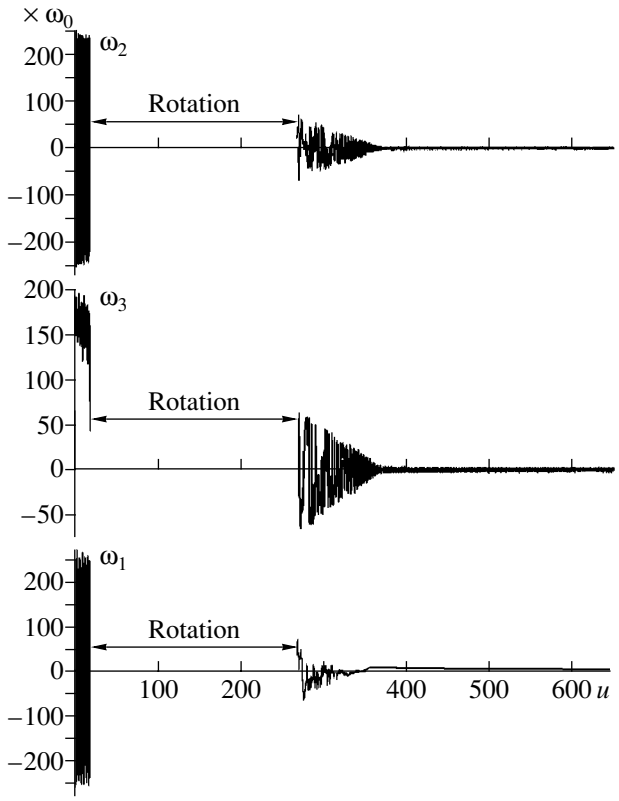

Fig. 11. Projections ω_1, ω_2, and ω_3 of the vector of absolute angular velocity onto the satellite's principal axis of inertia. The initial angular velocity is equal to $175\omega_0$ in each channel.

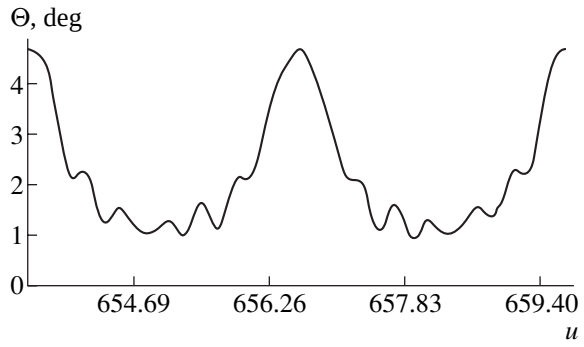

Fig. 12. The behavior of the Θ angle in the 105th orbit.

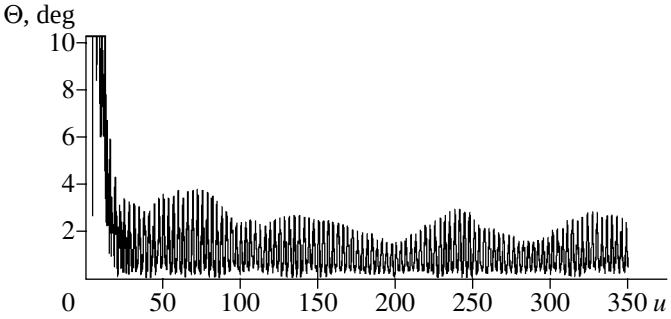

Fig. 13. The behavior of the Θ angle with the Earth's diurnal rotation taken into account.

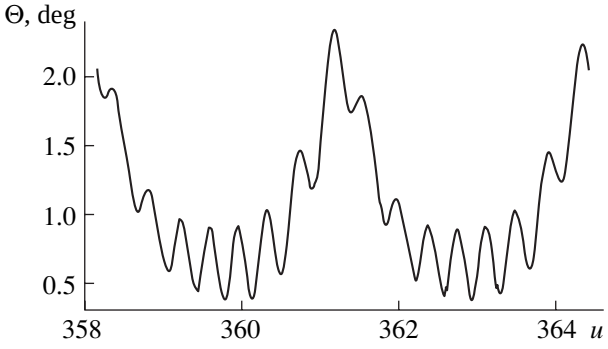

Fig. 14. The behavior of the Θ angle in a single orbit with the Earth's diurnal rotation taken into account.

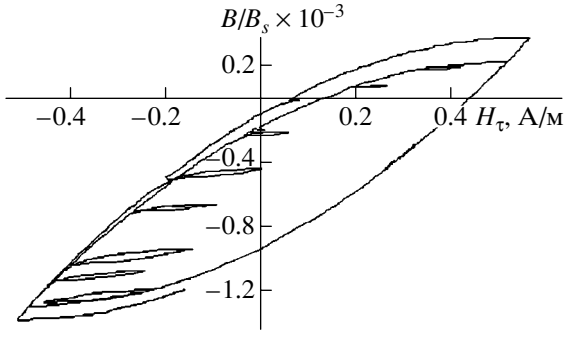

Fig. 15. The behavior of magnetization in an orbit for a rod along the Ox_3 axis.

$$\begin{pmatrix} 0.05283 & -0.0000678 & -0.0000230 \\ -0.0000678 & 0.05053 & -0.0000459 \\ -0.0000230 & -0.0000459 & 0.05283 \end{pmatrix} [\text{kg m}^2].$$

The satellite was assumed to have a permanent magnet with a moment $m = 0.5$ A m^2 and two triples of rods with a length of 15.5 cm whose parameters are specified by the manufacturer's certificate (Table 3). The initial velocity of rotation is 10 deg/s or $175\omega_0$ in every channel, the orbit height is 705 km, and the orbit inclination is 98°. The input parameters necessary for numerical calculations using the *improved* model of hysteresis, in accordance with the characteristics given above (Table 3), have the following values for each triple of rods: $k = 0.11$, $a = 0.17$, and $R_s = 4.6$.

Figure 10 with a plot of the Θ angle and Fig. 11 with projections of angular velocities ω_1, ω_2, and ω_3 present an example of the transition process. The plots are drawn starting from the moment preceding the transition from rotation to oscillations with respect to vector **H**. The dimensionless time u is reckoned from the moment of satellite separation from a carrier launcher. The plot for the Θ angle at the 105 orbit is scaled-up in Fig. 12. In approximately 60 orbits (slightly less than four days) the satellite stopped rotating and settled into the mode of oscillations with respect to vector **H** with an amplitude of about 20°. As in previous variants, the rate of further reduction of this amplitude is determined by the decreasing axial velocity of rotation. In the 105th orbit, the amplitude of oscillations has reduced to 4.7° at an angular rotation velocity of about $3\omega_0$, which has a tendency to further reduction. There was concern that the efficiency of rods with a loop narrower (Table 3) in comparison with that of GOST (Table 5) would be lower, but it turned out to be needless.

5.3. Inclusion of Daily Rotation of the Earth

The above results were obtained in the context of the *right dipole model*, according to which the field of a dipole antiparallel to the Earth's rotation axis and placed in the Earth's center approximates the geomagnetic field. Moreover, the angle between the dipole and its projection onto the orbit plane is invariant with time. When no hysteresis takes place, the equations of motion for a satellite depend on time periodically. This period is equal to the period of the satellite's revolution in orbit. It is precisely under this assumption that the periodic satellite motions whose amplitudes are presented in Fig. 5 were calculated. Under conditions of hysteresis, the system of equations does not apparently admit periodic solutions and one has to construct limiting regimes by integration over sufficiently long time intervals.

The right dipole model is obtained by simplifying the first approximation in the expansion of the geomagnetic field potential. In reality, the first approximation

describes the field of a *inclined dipole*, which is inclined to the Earth's rotation axis by approximately 11.5°. As a result of the diurnal rotation of the Earth, the angle between the dipole and its projection onto the orbit plane is continuously variable. The influence of this effect on the Θ angle is shown in Fig. 13. The initial conditions were chosen in such a way that the transition period would not take too long a time. Therefore, this figure is aimed at demonstrating the time behavior for the angle under nearly steady-state regimes and not the duration of the transition process. The time dependence is periodic with a period equal to approximately 16 orbits ($\Delta u \sim 100$), which comprises one day. The parameters of the satellite, magnet, and rods were taken as before. The time dependence of the Θ angle is shown in Fig. 14 for one revolution about the Earth.

Figure 15 presents the rod magnetization along the Ox_3 axis perpendicular to the orientation axis versus the projection of the vector of geomagnetic field strength onto the rod. In this case, the magnetization is normalized to the saturation induction equal to 0.74 T. Partial loops correspond to reverse magnetization of the rod under forced oscillations with frequencies close to the satellite's natural frequency. To describe the hysteresis model was not among the aims of this paper, but the above investigations demonstrated a good agreement of the experimental and calculated magnetization curves when the *improved model* was used. Most importantly, this agreement is observed for partial and nonsymmetric hysteresis loops. The parameters of the model given above (k, a, and R_s) are calculated using the geometrical and magnetic parameters of the rods [12].

5.4. Gaussian Model of the Geomagnetic Field

Now let us give an example of calculations made using the Gaussian IGRF-95 model with extrapolation of the coefficients to December 1999. Figure 16 presents the behavior of the angle Θ for two orbits when the transition process is nearly finished. In order to save calculation time, the initial velocity of the angular motion here was chosen to be considerably lower than its nominal value. Naturally, these results are distinct from those obtained with the models of right and inclined dipoles. However, one can consider the results to be in satisfactory agreement both qualitatively (the presence of two characteristic times equal to half an orbit and a period of natural oscillations) and quantitatively (the value of the maximum deviation in an orbit).

It should be emphasized that, among other things, the above preliminary and final calculations allowed us to estimate the degree of *coarseness* of our results with respect to the rod parameters that are controlled in the process of manufacturing with a fairly low accuracy. This is because only indirect methods of measuring the magnetic properties of materials are applied. The above calculations with different values of the rod parameters (both GOST and certified parameters) demonstrate a tolerable coarseness of results.

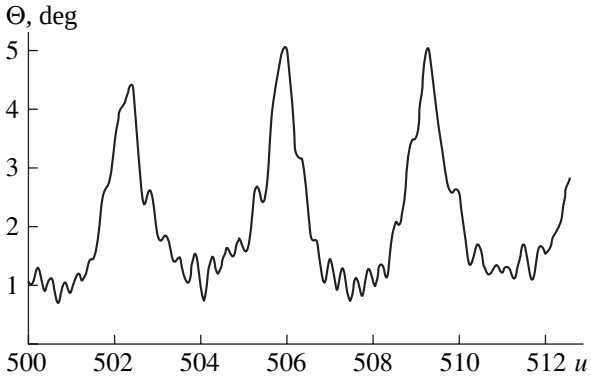

Fig. 16. The behavior of the Θ angle in two orbits for the Gaussian model of the geomagnetic field.

ACKNOWLEDGMENTS

This work was supported by the Institute of Space Physics (Sweden), by the Russian Foundation for Basic Research (projects no. 97-01-00910 and no. 00-01-00174), and by the Federal Special-Purpose Program "Integratsiya" (project no. A0110). We thank O. Norberg and S. Barabash for useful discussions and N. Fedoseev who consulted us about magnetically soft materials.

REFERENCES

1. Ovchinnikov, M., Penkov, V., Norberg, O., and Barabash, S., Attitude Control System for the First Swedish Nanosatellite *MUNIN*, *Acta Astronautica*, 2000, vol. 46, nos. 2–6, pp. 319–326.
2. Ovchinnikov, M.Yu., Small Satellites in Russia: Economy and Organization Aspects, in *Aktual'nye problemy aviatsionnykh i kosmicheskikh sistem* (Topical Problems of Aircraft and Spacecraft Systems), Kazan': Kazansk. Tekhn. Univ. & Aeronautical Univ. (Daytona Beach, USA), 1998, no. 1(5), pp. 13–25.
3. Sarychev, V.A. and Ovchinnikov, M.Yu., Magnetic Attitude Control Systems for Earth's Satellites, *Itogi Nauki Tekh., Ser.: Issled. Kosm. Prostr.*, vol. 23, Moscow: VINITI, 1985.
4. Ovchinnikov, M.Yu., Transient Motions of a Satellite with a Magnetic Attitude Control System in the Framework of a Simple Model of Hysteresis, *Kosm. Issled.*, vol. 38, no. 1, pp. 78–84.
5. Sarychev, V.A. and Ovchinnikov, M.Yu., Attitude Motion of a Satellite with a Permanent Magnet, *Kosm. Issled.*, 1986, vol. 24, no. 4, pp. 527–543.
6. King, J.A., McGwier, R., Price, H., and White, J., The In-Orbit Performance of Four Microsat Spacecraft, *Paper of AIAA/USU Conference on Small Satellites, Utah, US*, 1990.
7. Agapov, V., Eleven Satellites in Orbits as a Result of an Experimental Launch, *Novosti Kosmonavtiki*, 2000, no. 2, pp. 10–16.

8. Plotnikov, V.A. and Zverkova, T.S., Method of Averaging for Systems of a Standard Type with Discontinuous Right Hand Sides, *Differents. Uravn.*, 1982, vol. 18, no. 6, pp. 1076–1078.
9. Ovchinnikov, M.Yu., Application of Hysteresis Rods in Magnetic Attitude Control Systems for Satellites, in *Aktual'nye problemy prikladnoi nebesnoi mekhaniki. Trudy XIV Nauchnykh Chtenii po kosmonavtike* (Topical Problems of Applied Celestial Mechanics, Proc. XIV Science Readings in Astronautics), Moscow: IIET, 1990, p. 14.
10. Pivovarov, M.L., Oscillations of a Satellite with Magnetic Stabilization, *Preprint of Space Res. Inst., Russ. Acad. Sci.*, Moscow, 1990, Pr.-1685.
11. Kovalenko, A.P., *Magnitnye sistemy upravleniya kosmicheskimi letatel'nymi apparatami* (Magnetic Control Systems for Spacecraft), Moscow: Mashinostroenie, 1975.
12. Sarychev, V.A., Pen'kov, V.I., and Ovchinnikov, M.Yu., A Mathematical Model of Hysteresis Based on a Magnetomechanical Analogy, *Mat. Model.*, 1989, vol. 1, no. 4, pp. 122–133.
13. Ovchinnikov, M.Yu. and Pen'kov, V.I., Investigation of Damping Properties of Magnetic Hysteresis Rods with Taking Their Mutual Reversal Magnetization into Account, in *Prikladnaya mekhanika i matematika* (Applied Mechanics and Mathematics), Moscow: Mosk. Fiz.-Tekh. Inst., 1992, pp. 104–110.
14. Horn, G. and Regenberg, S., Zur Stabilisierung Eines Satelliten mit Hilfe des Erdmagnetfeifdes, *Z. Flugwiss.*, 1966, vol. 14, no. 9, pp. 398–413.